

Collective excitations in a superfluid of color-flavor locked quark matter

Kenji Fukushima^{1,2} and Kei Iida³

¹*Center for Theoretical Physics, Massachusetts Institute of Technology, Cambridge, Massachusetts 02139, USA*

²*Department of Physics, University of Tokyo, 7-3-1 Hongo, Bunkyo-ku, Tokyo 113-0033, Japan*

³*RIKEN BNL Research Center, Brookhaven National Laboratory, Upton, New York 11973-5000, USA*

We investigate collective excitations coupled with baryon density in a system of massless three-flavor quarks in the collisionless regime. By using the Nambu–Jona-Lasinio (NJL) model in the mean-field approximation, we field-theoretically derive the spectra both for the normal and color-flavor locked (CFL) superfluid phases at zero temperature. In the normal phase, we obtain usual zero sound as a low-lying collective mode in the particle-hole (vector) channel. In the CFL phase, the nature of collective excitations varies in a way dependent on whether the excitation energy, ω , is larger or smaller than the threshold given by twice the pairing gap Δ , at which pair excitations with nonzero total momentum become allowed to break up into two quasiparticles. For $\omega \ll 2\Delta$, a phonon corresponding to fluctuations in the $U(1)$ phase of Δ appears as a sharp peak in the particle-particle (“ H ”) channel. We reproduce the property known from low energy effective theories that this mode propagates at a velocity of $v_H = 1/\sqrt{3}$ in the low momentum regime; the decay constant f_H obtained in the NJL model is identical with the QCD result obtained in the mean-field approximation. We also find that as the momentum of the phonon increases, the excitation energy goes up and asymptotically approaches $\omega = 2\Delta$. Above the threshold for pair excitations ($\omega > 2\Delta$), zero sound manifests itself in the vector channel. By locating the zero sound pole of the vector propagator in the complex energy plane we investigate the attenuation and energy dispersion relation of zero sound. In the long wavelength limit, the phonon mode, the only low-lying excitation, has its spectral weight in the H channel alone, while the spectral function vanishes in the vector channel. This is due to nontrivial mixing between the H and vector channels in the superfluid medium. We finally extend our study to the case of nonzero temperature. We demonstrate how Landau damping smears the phonon peak in the finite temperature spectral function. We find a pure imaginary pole of the H propagator in the complex energy plane, which can be identified as a diffusive mode responsible for the Landau damping. From the pole position we derive the thermal diffusion constant.

PACS numbers: 12.38.-t, 25.75.Nq

I. INTRODUCTION

Quark matter at high baryon density is considered to have a rich phase structure in a way dependent on the physical conditions for color and flavor such as weak equilibrium and color neutrality. For the past few decades it has been predicted that cold quark matter is color superconducting when the baryon density is sufficiently high [1]. Color superconductivity occurs in quark matter in a similar manner to ordinary superconductivity in metals; any attractive force between quarks can bring about an instability of the Fermi surface against Cooper pairing, which subsequently leads to a BCS superfluid state characterized by condensation of quark Cooper pairs and to a color version of the Meissner effect through nonvanishing color charge carried by the pairs. In fact, the quark-quark force induced by one-gluon exchange is attractive in the color antisymmetric channel. At asymptotically high densities where the interactions are dominated by one-gluon exchange, this attractive force should drive Cooper instability. More recently, effective model analyses, rather than rigorous QCD calculations, have predicted that quark matter is a color superconductor even at several times normal nuclear density and that the zero temperature pairing gap and thus the critical temperature are of order 10–100 MeV.

In possible physical realizations in heavy ion collisions

and neutron stars, color superconducting quark matter might leave evidences for color superconductivity via precursory phenomena above the critical temperature [2], neutrino emission from proto-neutron stars [3], and neutron star cooling [4, 5], etc. To obtain such possible evidences, it is indispensable to clarify the equilibrium properties of color superconductors such as the equation of state and elementary excitations. This paper elaborates on collective excitations in quark matter, which might help us detect the onset of color superconductivity.

Since quarks have more internal degrees of freedom than electrons by two (color and flavor), various pairing patterns are possible among quarks, even within a state of S -wave, spin-singlet pairing. The ratio between the strange quark mass and the quark chemical potential is known to be a crucial parameter that determines the energetically favorable pairing pattern. In the case of three massless flavors the color-flavor locked (CFL) phase [6] is the ground state [7]. In this paper we shall focus only on the massless limit of CFL quark matter in which the baryon number conservation is spontaneously broken by the condensation of quark pairs. This can be mathematically formulated as global $U(1)_B$ symmetry breaking, as we briefly recapitulate in Sec. II.

Superfluid ${}^3\text{He}$, a typical laboratory fermion system that exhibits global $U(1)$ symmetry breaking [8], is similar to CFL quark matter in many respects. In fact, the

ground state of liquid ${}^3\text{He}$, i.e., the B phase, has a condensate *isotropic* in spin-orbit space, which is similar to the CFL phase in which the condensate is *isotropic* in color-flavor space. In both systems, responses to rotation are characterized by a lattice of vortices [9].

In the B phase of superfluid ${}^3\text{He}$ in which the pairing gap has no nodes, thermal quasiparticle excitations are suppressed at temperatures much lower than the gap. In this case, the thermodynamic properties such as the specific heat are presumably controlled by phonon excitations, Nambu-Goldstone bosons corresponding to fluctuations in the $U(1)$ phase of the pairing gap, which appear in the low energy spectral function in the particle-particle channel. Then, the same kind of phonons in CFL matter (often denoted by H) are expected to play a key role in the thermodynamic properties at low temperatures [10, 11]. In this paper we investigate the H phonon spectrum in the energy range including the scale beyond the pairing gap Δ in the random phase approximation of a Nambu–Jona-Lasinio (NJL) model for CFL quark matter. This microscopic approach enables us to see that H , if embedded in the quasiparticle continuum lying above 2Δ , would decay into two quasiparticle quarks.

We remark that an H mode does not appear as a transverse mode, a feature responsible for a nonzero value of the superfluid baryon density at zero temperature [12]. Transverse excitations will be ignored in the present study, but play a role in breaking up phase coherence in the superfluid state and hence are relevant for responses to magnetic field and rotation [9, 13] and for reduction in the transition temperature [14].

In normal quark matter we also describe zero sound as fluctuations in the baryon density by analyzing the spectral function in the particle-hole (vector) channel in the random phase approximation in which collisions between quark quasiparticles are ignored (see Ref. [15] for general arguments of relativistic zero sound). We extend the description of zero sound to the case of the CFL phase. We find that in the vector channel, zero sound manifests itself as an attenuated mode in the quasiparticle continuum lying above twice the gap, while H dominates the spectrum below the continuum. We remark that for general excitation momenta the random phase approximation is strictly applicable to weakly coupled systems. In this respect, a recent observation of zero sound in the lattice simulation based on a QCD-like model [16] is noteworthy.

Note that in the collisionless regime the restoring force of the collective modes is a self-consistent field formed by a number of particles, which would be disrupted by interparticle collisions if any. Collective modes in the hydrodynamic regime such as first sound, of which the restoring force is provided by the collisions, will be addressed in our future study. For the study of low-lying collective modes in both regimes, the Landau theory of Fermi liquids is useful. This is the case with normal liquid ${}^3\text{He}$ [17], superfluid ${}^3\text{He}$ [18], and normal quark matter [19].

In calculating the spectral functions in the CFL phase,

it is important to take into account the mixing between the particle-particle and particle-hole channels. This is because such mixing plays a role in determining the spectral weight of H and zero sound modes. We find that in the long wavelength limit the spectral function in the particle-hole channel vanishes due to the mixing effect.

We summarize the main conclusions of this paper as follows:

- The velocity of the H mode in the small momentum regime is $1/\sqrt{3}$ at zero temperature. As the momentum goes up, the mode energy monotonically approaches 2Δ , above which individual pair excitations are kinematically allowed. The velocity $1/\sqrt{3}$ corresponds to the ratio of the spatial and temporal components of the decay constant f_H . We find that the expression for f_H in the NJL model adopted here is the same as the QCD result in the mean-field approximation.
- In the CFL phase zero sound appears as an attenuated mode in the quasiparticle continuum extending above 2Δ . The attenuation width decreases with increasing momentum.
- In the CFL phase, the spectral function in the vector channel is strongly suppressed at small momenta by the mixing with the particle-particle channel.
- At finite temperature at which thermally excited quasiparticles are present, the H mode has a finite decay width due to Landau damping. Correspondingly, a pure imaginary pole appears in the H propagator. We estimate the thermal diffusion constant from the pole behavior in the complex energy plane.

We note that the present work, which focuses on collective modes coupled with baryon density fluctuations in the CFL phase, is a complement to the work by Gusynin and Shovkovy [20] that gave a detailed account of collective modes coupled with color current fluctuations in the CFL phase.

This paper is organized as follows: We briefly review the CFL Cooper pairing and the symmetry breaking pattern in Sec. II. We describe a model for quark matter, the self-consistency equations, and the spectral functions in Sec. III. Full expressions for the spectral functions are listed in Appendix A. Section IV is devoted to showing the results for H and zero sound modes at zero temperature. In Sec. V, we present the results at finite temperature and discuss Landau damping of the H mode. Concluding remarks are given in Sec. VI. Appendix B explains how we perform the analytic continuation of the propagators of collective excitations to search for the poles in the complex energy plane. We work in units $\hbar = c = k_B = 1$.

II. COOPER PAIRING, SYMMETRY BREAKING, AND NAMBU-GOLDSTONE BOSONS

In this section, we summarize the fundamental properties of the CFL phase. In particular, the symmetry breaking pattern and the associated Nambu-Goldstone bosons are mentioned.

In the CFL phase with uds -flavor and RGB -color massless quarks, the energetically favored Cooper pairing of quarks is antisymmetric in color space and has even parity and zero total angular momentum [6, 7]. Then, the antisymmetry of the pairing in flavor space follows from the Pauli principle. [Note that in the absence of quark masses, only quarks of the same chirality can be paired [21].] The corresponding diquark condensate reads

$$\langle \bar{\psi}_{\alpha i}^C \gamma_5 \psi_{\beta j} \rangle \sim \Delta (\delta_{\alpha i} \delta_{\beta j} - \delta_{\alpha j} \delta_{\beta i}), \quad (1)$$

where the Roman and Greek subscripts stand for the indices in flavor and color space, respectively, ψ is the quark spinor, and $\psi^C = C\bar{\psi}^T$ is the charge conjugate spinor with the charge conjugation matrix $C = i\gamma^2\gamma^0$ in the Pauli-Dirac representation. A precise relation between the condensate and the pairing gap will be given in Eq. (5) after introducing a model for quark matter. The coexisting condensate in the CFL phase, which arises in a color and flavor symmetric state, will be ignored since it makes negligible difference in the present analysis that focuses on the superfluid properties.

The condensate (1) breaks both $SU(3)_L$ and $SU(3)_R$ of chiral symmetry, whereas it leaves unbroken a symmetry under a vector rotation in flavor space and a simultaneous color rotation in the opposite orientation. The symmetry breaking pattern in the CFL phase can thus be written as [1, 6]

$$[SU(3)_{\text{color}}] \times SU(3)_L \times SU(3)_R \times U(1)_B \\ \rightarrow SU(3)_{C+L+R} \times \mathbb{Z}_2.$$

Here, \mathbb{Z}_2 is a symmetry under $\psi \rightarrow -\psi$. Nine Nambu-Goldstone bosons result from the spontaneous symmetry breaking described above. Eight pion-like bosons associated with the breakdown of the axial part of chiral symmetry form an octet in $SU(3)_{C+L+R}$ just like (π, K, η) in hadronic matter. One more massless boson arises as a color-flavor singlet from the spontaneous breaking of baryon number conservation in a manner that preserves local electric and color charge neutrality. This singlet boson is a phonon (often referred to as H) corresponding to $U(1)_B$ phase fluctuations of the condensate (1).

For completeness, let us consider the other phases which are predicted to appear in the phase diagram for neutral quark matter with nonzero strange quark mass [22, 23, 24] and confirm that all these phases do not have an H mode. It is well known that in the 2SC phase in which only two colors and two flavors participate in pairing, there remains an unbroken baryon number symmetry associated with the unpaired color and flavor. In

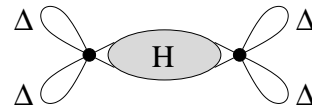


FIG. 1: Schematic picture of the H propagation. Colored diquark condensates supply color charge in such a way as to make H a color singlet at the edges.

the same way, the uSC and dSC phases in which only ds and us pairing is breached as compared with the pairings in the CFL phase, respectively, preserve a modified $U(1)_B$ symmetry. The uSC phase, for instance, has finite condensates $\langle ud \rangle$ and $\langle su \rangle$. These two condensates are invariant simultaneously under rotations generated by an appropriate linear combination of the $U(1)_B$ generator and two $U(1)$ generators corresponding to flavor number conservation. Therefore, there is no H in the 2SC, uSC, and dSC phases. Put another way, in each of these phases, $U(1)_B$ phase fluctuations in the order parameter are inevitably coupled with electric and color charge density since the condensates, as a whole, are not charge neutral in electricity and color. We note that in the CFL phase modified by quark masses different among flavors, H modes could be affected by coupling with electric and color charge density. In this case, the quark system, if being color neutral and being neutralized and β -equilibrated by an electron gas, would generally have a superfluid part that is no longer charge neutral in electricity and/or color. This nonneutral superfluid part would occur not only at nonzero temperature, but also in the presence of gapless quark modes even at zero temperature [25].

All the Nambu-Goldstone bosons in the CFL condensate (1) are color singlets because the corresponding fluctuations in the order parameter are not coupled with color charge density and thus are not eaten by the longitudinal component of color gauge fields through the Anderson-Higgs mechanism. It follows that the CFL pions and H consist of at least four and six quarks, respectively [26], i.e., they are composed of such combinations of particle-particle and hole-hole pairs as $(RG)(\bar{R}\bar{G})$ and $(RG)(GB)(BR)$. In this paper we assume that colored diquark condensates compensate color charge at the edges of the H propagator as shown in Fig. 1. We can then describe the propagating part of H by a state having an excited quark Cooper pair in Fock space. This picture is based on a mean-field approximation, which is valid as long as the size of the mean-field Δ is larger than the size of quantum and thermal fluctuations around Δ .

III. MODEL CALCULATIONS

In this section we first describe the equilibrium properties of a normal fluid and a superfluid of quark matter with three massless flavors by utilizing an effective model with local four-quark interactions. We then ex-

amine excitation spectra in both phases in the random phase approximation.

A. Self-consistency equations

We begin with a model for massless three-flavor quark matter. For the later purpose of describing collective excitations in the particle-particle (H) and particle-hole (vector) channels, it is convenient to deal with the Lagrangian density having the diquark and vector interactions. One can generally obtain such interaction terms from any local four-quark interactions after appropriate Fierz transformation. Then the Lagrangian density can be written as

$$\mathcal{L} = \bar{\psi}(i\cancel{\partial} + \mu_q\gamma^0)\psi + \mathcal{L}_D + \mathcal{L}_V, \quad (2)$$

where μ_q is the quark chemical potential, \mathcal{L}_D and \mathcal{L}_V are the diquark and vector interaction terms as will be specified below. As we will see later, μ_q receives a finite correction from the vector mean-field. Hereafter we will take $\mu_q = 500$ MeV. The corresponding baryon density is, as we will see later, approximately $10\rho_0$ in our calculation where $\rho_0 \simeq 0.16 \text{ fm}^{-3}$ is the normal nuclear density, and may be relevant in the cores of compact stellar objects, although ideally symmetric CFL quark matter as considered here is only relevant at much higher densities where the strange quark mass is negligibly small compared with the quark chemical potential. Note, however, that we have technical difficulty in taking an extremely large value of μ_q , because the effective model with the interaction terms that will be shown below is non-renormalizable and needs a finite cut-off parameter, Λ . We shall choose $\Lambda = 1$ GeV in this paper. Then, our choice, $\mu_q = 500$ MeV, can be considered effectively as the upper limit at which quark excitations around the Fermi surface would hardly suffer from any cut-off artifact. We thus expect that our analysis of collective excitations with momenta up to ~ 100 MeV is free from such artifact.

In this paper, for simplicity, we choose \mathcal{L}_D to be the interaction that occurs only in the color-flavor singlet diquark channel. This ansatz for \mathcal{L}_D makes no difference in the resulting gap equations as far as ideally symmetric CFL quark matter is concerned. The four-quark interactions thus take the following forms:

$$\mathcal{L}_D = \frac{G}{12}(\bar{\psi}_{\alpha i}P_{\alpha\beta}^{ij}\psi_{\beta j}^C)(\bar{\psi}_{\alpha' i'}P_{\alpha'\beta'}^{i'j'}\psi_{\beta' j'}^C), \quad (3)$$

$$\mathcal{L}_V = -\frac{G_V}{2}(\bar{\psi}\gamma_\mu\psi)(\bar{\psi}\gamma^\mu\psi), \quad (4)$$

with $P_{\alpha\beta}^{ij} = i\gamma_5\epsilon^{ijk}\epsilon_{\alpha\beta k}$ in which the sum is taken over k .

The value of G_V is of the order of G , but our qualitative results for elementary excitations are independent of a particular choice of G_V . Hereafter we shall take $G_V = G/2$ for definiteness. A different G_V provides a different (dimensionless) spectral weight in the vector

channel, which is approximately scaled by G_V unless G_V is anomalously large.

It should be emphasized that the vector interaction generally arises since chiral symmetry is intact; \mathcal{L}_V is chirally symmetric itself. For specific values of G_V the phase diagram on the temperature versus chemical potential plane can have such intricate structures as to contain multiple critical end-points associated with diquark and chiral condensates [27]. Since the density region of interest here is presumably beyond the chiral transition density, we simply ignore effects of chiral condensation.

As to the diquark interaction, we shall fix G in such a way that the solution to the self-consistency equations with $G_V = G/2$ yields $\Delta = 25$ MeV with $\mu_q = 500$ MeV at zero temperature. As we will see in Sec. IV, the properties of collective excitations in the CFL state change drastically according to whether they reside above or below 2Δ , which corresponds to a threshold above which pair excitations are allowed to occur. As long as Δ is much smaller than the quark chemical potential and much larger than the temperature, the energy and momentum of collective excitations are essentially scaled by Δ . In this case, a single example presented here with the choice $\Delta = 25$ MeV suffices for us to deduce what takes place for general values of Δ .

Let us proceed to adopt the mean-field approximation by introducing variational variables, i.e., the gap parameter, Δ , and the quark number density, n_q , as

$$\Delta = \frac{G}{6}\langle\bar{\psi}_{i\alpha}P_{\alpha\beta}^{ij}\psi_{j\beta}^C\rangle, \quad (5)$$

$$n_q = \langle\bar{\psi}\gamma^0\psi\rangle. \quad (6)$$

As we shall see, we obtain the self-consistency equations that determine these variables by substituting the mean-field quark propagator with Δ and n_q into the right side of Eqs. (5) and (6). Equivalently, these self-consistency equations can be obtained from the stationary conditions on the mean-field thermodynamic potential with respect to Δ and n_q . The corresponding equations are the gap equation and the relation between the quark density and chemical potential.

It is well known that the mean-field quark propagator in the CFL phase takes the simplest form in the CFL basis, $\psi_{\alpha i} = (\lambda^A/\sqrt{2})_{\alpha i}\psi^A$ and $\bar{\psi}_{\alpha i} = \bar{\psi}^A(\lambda^A/\sqrt{2})_{i\alpha}$. Here, the matrices, λ^A , in color-flavor space are the Gell-Mann matrices for $A = 1, \dots, 8$ and $(\lambda^0)_{i\alpha} = \sqrt{2/3}\delta_{i\alpha}$ for $A = 0$, which are normalized as $\frac{1}{2}\text{tr}\lambda^A\lambda^B = \delta^{AB}$. In the CFL basis, the gap matrix in the quark propagator, $\Delta P_{\alpha\beta}^{ij}$, has only diagonal components, i.e., $i\gamma_5\text{diag}\{\Delta_A\}$, where $\Delta_A = -\Delta$ for an octet in color-flavor space ($A = 1, \dots, 8$) and $\Delta_A = 2\Delta$ for a singlet ($A = 0$).

In the present analysis of the self-consistency equations, one is not allowed to simplify calculations by dropping the antiparticle part in the quark propagator. This is because the cancellation between the particle and antiparticle contributions for momenta above the Fermi surface is crucial for the evaluation of n_q in the NJL model. At zero temperature, as a first approximation, one can

estimate n_q from the number density in a free quark gas as $3\mu_q^3/\pi^2 = 4.9 \text{ fm}^{-3}$ for $\mu_q = 500 \text{ MeV}$, which corresponds to a baryon density of roughly $10\rho_0$ as we have mentioned before. The NJL model calculation including both the particle and antiparticle contributions results in $n_q = 5.1 \text{ fm}^{-3}$ for $\mu_q = 500 \text{ MeV}$ with $\Delta = 25 \text{ MeV}$. This is consistent with the first estimate, while we obtain $n_q = -14.7 \text{ fm}^{-3}$ in the absence of the antiparticle contribution; even the sign is inconsistent.

It is a usual technique to decompose the quark propagator into the particle and antiparticle parts by using the energy projection operators of noninteracting massless quarks, $\Lambda_p^\pm = \frac{1}{2}(1 \pm \gamma^0 \vec{\gamma} \cdot \hat{p})$, where $\hat{p} = \vec{p}/p$. Using these operators, we can explicitly write down the mean-field quark propagator in 2×2 Nambu-Gor'kov space as

$$S_{AB}(p^\mu) = \delta_{AB} \gamma^0 \left\{ \begin{bmatrix} \Lambda_p^- & 0 \\ 0 & \Lambda_p^+ \end{bmatrix} S_A^p + \begin{bmatrix} \Lambda_p^+ & 0 \\ 0 & \Lambda_p^- \end{bmatrix} S_A^a \right\}, \quad (7)$$

where the particle part is

$$S_A^p(p^\mu) = \frac{i}{p_0^2 - (\epsilon_{\Delta_A}^-)^2} \begin{bmatrix} p_0 + (p - \mu_r) & -i\Delta_A \gamma_5 \gamma^0 \\ -i\Delta_A \gamma_5 \gamma^0 & p_0 - (p - \mu_r) \end{bmatrix}, \quad (8)$$

the antiparticle part is

$$S_A^a(p^\mu) = \frac{i}{p_0^2 - (\epsilon_{\Delta_A}^+)^2} \begin{bmatrix} p_0 - (p + \mu_r) & -i\Delta_A \gamma_5 \gamma^0 \\ -i\Delta_A \gamma_5 \gamma^0 & p_0 + (p + \mu_r) \end{bmatrix}, \quad (9)$$

and we have chosen the Nambu-Gor'kov basis as

$$\bar{\Psi}(p^\mu) = [\bar{\psi}(p^\mu), \bar{\psi}^C(-p^\mu)], \quad \Psi(p^\mu) = \begin{bmatrix} \psi(p^\mu) \\ \psi^C(-p^\mu) \end{bmatrix}. \quad (10)$$

Here we have defined the energy of quark and antiquark quasiparticles as $\epsilon_{\Delta_A}^\pm = \sqrt{(p \pm \mu_r)^2 + \Delta_A^2}$ and the quark chemical potential renormalized by the vector interaction term as

$$\mu_r = \mu_q - G_V \cdot n_q, \quad (11)$$

which amounts to $\mu_r = 434.7 \text{ MeV}$ for our parameter choice at zero temperature.

We can finally obtain the self-consistency equations at given temperature T by substituting the off-diagonal and diagonal components of S_{AB} given by Eq. (7) into the right side of Eqs. (5) and (6), respectively. Here we set $p_0 = in\pi T$ and take the Matsubara frequency sum over

odd n . The results read

$$1 - \frac{G}{3\pi^2} \int^\Lambda dp p^2 \left[\frac{2}{\epsilon_{\Delta}^-} \tanh\left(\frac{\epsilon_{\Delta}^-}{2T}\right) + \frac{1}{\epsilon_{2\Delta}^-} \tanh\left(\frac{\epsilon_{2\Delta}^-}{2T}\right) + (\text{same with } \epsilon^- \rightarrow \epsilon^+) \right] = 0, \quad (12)$$

$$n_q - \frac{1}{2\pi^2} \int^\Lambda dp p^2 \left[\frac{8\partial\epsilon_{\Delta}^-}{\partial\mu_r} \tanh\left(\frac{\epsilon_{\Delta}^-}{2T}\right) + \frac{\partial\epsilon_{2\Delta}^-}{\partial\mu_r} \tanh\left(\frac{\epsilon_{2\Delta}^-}{2T}\right) + (\text{same with } \epsilon^- \rightarrow \epsilon^+) \right] = 0. \quad (13)$$

The first term in the square brackets is the particle contribution from octet quarks; the second from singlet quarks. The antiparticle contributions lead to the same expressions as the particle contributions with ϵ^- replaced by ϵ^+ .

We determine G and μ_r from Eqs. (11), (12), and (13) in such a way that the solutions to these equations yield $\Delta = 25 \text{ MeV}$ with $\mu_q = 500 \text{ MeV}$ at zero temperature, as we have explained above. Once we fix the model parameters at zero temperature, we can derive the temperature dependence of Δ and μ_r from the same equations. Such self-consistency equations predict a second-order phase transition from the CFL phase to unpaired quark matter at $T_c = 18.15 \text{ MeV}$. This value of T_c is larger than the BCS value of $\simeq 0.57\Delta$ due to the two-gap structure of the quark excitations ($-\Delta$ and 2Δ for octet and singlet quarks, respectively) [28]. We note, however, that in a situation in which CFL quark matter behaves as a type-I color superconductor, thermal fluctuations in the gauge fields could play a role in changing the phase transition from second to first order and in lowering the transition temperature [14]. The analysis of this situation is beyond the scope of the present paper. In Sec. V, we will present the finite temperature results showing an appreciable Landau damping effect on H modes at $T = 0.8T_c$, under the expectation that CFL quark matter at $T = 0.8T_c$ is not affected severely by thermally fluctuating gauge fields.

B. Collective excitations

We proceed to describe longitudinal collective excitations in a superfluid as well as in a normal fluid of quark matter in the random phase approximation. The collective modes that we can describe in this approximation are an H phonon in the particle-particle channel and zero sound in the particle-hole channel, and they lie in the collisionless regime.

In the random phase approximation, as we have briefly noted in Sec. II, we can assume that for H modes, color singletness is achieved at the edges of the propagator (see Fig. 1). We can thus regard such collective excitations as an excited Cooper pair with nonzero total momen-

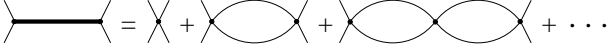


FIG. 2: Schematic diagrams representing the propagation of collective excitations.

tum that multiply scatter with each other in a superfluid medium, instead of considering the propagation of three excited Cooper pairs. We can likewise consider zero sound in terms of the propagation of a quark particle-hole pair both in a normal and a superfluid medium. Consequently, the propagator of collective excitations can be expressed as a sum over the bubble diagrams in the corresponding channel as exhibited in Fig. 2. In this subsection we construct the vertices from the interaction terms in the H and vector channels and compute the bubble diagrams.

Let us now construct matrices, Γ , at the vertices from the interaction terms. In doing so, we first rewrite the four-quark interactions in terms of the Nambu-Gor'kov basis. This is straightforward although we should pay attention to how to count the Nambu-Gor'kov replicas. Since collective excitations couple not only with the original fields but also with the replica fields, the four-quark interactions in terms of the Nambu-Gor'kov basis involve the original ones, the replica copies, and the original-replica cross terms. The resultant diquark interaction is

$$\begin{aligned} \mathcal{L}_D &\rightarrow 4 \times \mathcal{L}_D \\ &= \frac{G}{12} \left[(\bar{\psi}_{\alpha i} P_{\alpha\beta}^{ij} \psi_{\beta j}^C + \bar{\psi}_{\alpha i}^C P_{\alpha\beta}^{ij} \psi_{\beta j})^2 \right. \\ &\quad \left. - (\bar{\psi}_{\alpha i} P_{\alpha\beta}^{ij} \psi_{\beta j}^C - \bar{\psi}_{\alpha i}^C P_{\alpha\beta}^{ij} \psi_{\beta j})^2 \right] \\ &= \frac{G}{12} [(\bar{\Psi}_{\alpha i} \Gamma_{D\alpha\beta}^{+ij} \Psi_{\beta j})^2 + (\bar{\Psi}_{\alpha i} \Gamma_{D\alpha\beta}^{-ij} \Psi_{\beta j})^2], \end{aligned} \quad (14)$$

where

$$\Gamma_{D\alpha\beta}^{+ij} = \begin{bmatrix} 0 & P_{\alpha\beta}^{ij} \\ P_{\alpha\beta}^{ij} & 0 \end{bmatrix}, \quad \Gamma_{D\alpha\beta}^{-ij} = \begin{bmatrix} 0 & iP_{\alpha\beta}^{ij} \\ -iP_{\alpha\beta}^{ij} & 0 \end{bmatrix} \quad (15)$$

are the matrices associated with fluctuations in the amplitude and the $U(1)$ phase of the diquark condensate, respectively. We can likewise express the vector interaction as

$$\mathcal{L}_V \rightarrow 4 \times \mathcal{L}_V = -\frac{G_V}{2} (\bar{\Psi} \Gamma_{V\mu} \Psi) (\bar{\Psi} \Gamma_V^\mu \Psi) \quad (16)$$

with the matrix defined by

$$\Gamma_V^\mu = \begin{bmatrix} \gamma^\mu & 0 \\ 0 & -\gamma^\mu \end{bmatrix}. \quad (17)$$

By using the quark propagator (7) with the definitions (8) and (9) and the matrices (15) and (17), we can

express the bubble diagrams as

$$\begin{aligned} &\Pi_H(q_0, \vec{q}) \\ &= -\frac{i}{2} \int^T \frac{d^4 p}{(2\pi)^4} \text{tr} \Gamma_D^- S(p_0 + q_0, \vec{p} + \vec{q}) \Gamma_D^- S(p_0, \vec{p}), \end{aligned} \quad (18)$$

$$\begin{aligned} &\Pi_V^{\mu\nu}(q_0, \vec{q}) \\ &= -\frac{i}{2} \int^T \frac{d^4 p}{(2\pi)^4} \text{tr} \Gamma_V^\mu S(p_0 + q_0, \vec{p} + \vec{q}) \Gamma_V^\nu S(p_0, \vec{p}), \end{aligned} \quad (19)$$

$$\begin{aligned} &\Pi_M^\mu(q_0, \vec{q}) \\ &= -\frac{i}{2} \int^T \frac{d^4 p}{(2\pi)^4} \text{tr} \Gamma_D^- S(p_0 + q_0, \vec{p} + \vec{q}) \Gamma_V^\mu S(p_0, \vec{p}) \end{aligned} \quad (20)$$

for the H , vector, and H -vector mixed channels, respectively. Here, $\int^T d^4 p / (2\pi)^4$ denotes the integration over \vec{p} with the cut-off Λ and the Matsubara summation with respect to p_0 , and the trace is taken over color, flavor, spinor, and Nambu-Gor'kov indices. The factor 1/2 is necessary for adjusting the duplicate loop counting in the Nambu-Gor'kov basis.

In the present study we do not consider the bubble diagrams including the vertex Γ_D^+ associated with fluctuations in the amplitude of the order parameter. This is partly because collective amplitude modes are embedded in the quasiparticle continuum lying above 2Δ and heavily damped and partly because the important decay process of an amplitude mode into two H modes is beyond the reach of the random phase approximation.

We shall pick up only the $\mu = \nu = 0$ component of the bubble diagrams involved in the vector interaction, i.e., Π_V^{00} and Π_M^0 , while discarding the longitudinal spatial components of the bubble diagrams whose cut-off dependence is not well controllable in the NJL model [see discussions around Eq. (A3) for details.] These spatial components, even if taken into account, would only change zero sound from superluminal to subluminal and would not essentially change the H -vector mixing and the behavior of attenuated zero sound in the CFL phase, as we shall see in the next section.

We list the explicit expressions for Π_H , Π_V^{00} , and Π_M^0 in Appendix A. We shall omit the superscript “0” hereafter.

It is convenient to arrange the polarizations and the coupling constants in a matrix form

$$\mathbf{\Pi} = \begin{bmatrix} \Pi_H & \Pi_M \\ -\Pi_M & \Pi_V \end{bmatrix}, \quad \mathbf{G} = \begin{bmatrix} \frac{G}{12} & 0 \\ 0 & -\frac{G_V}{2} \end{bmatrix}. \quad (21)$$

It is clear from this form that we can analyze the H -vector mixing effect by picking up eigenmodes in the corresponding channel. It should be noted that we always mean by the H channel the channel corresponding to phase fluctuations of the Cooper pair and that H as a physical excitation appears in an eigen-channel given by a mixture of the H channel and the vector channel.

The retarded propagator as sketched in Fig. 2 is expressed in terms of $\mathbf{\Pi}$ and \mathbf{G} as

$$\mathbf{D}^R(\omega, \vec{q}) = \frac{1}{(2\mathbf{G})^{-1} - \mathbf{\Pi}(\omega + 0^+, \vec{q})}. \quad (22)$$

This propagator contains all information on the dynamics of collective excitations in the collisionless regime such as the mass, the attenuation width, and the energy dispersion relation. As a simple exemplification, let us briefly make sure how the propagator (22) is consistent with the presence of a massless H mode. In the limit of $\vec{q} = 0$ and $\omega \rightarrow 0$, the mixed diagram Π_M vanishes and the denominator of the H propagator reduces to $6/G - \Pi_H(0, 0)$. Note that this denominator is proportional to the left side of the gap equation (12). We thus find that it is zero given the explicit expression (A2). This means that the propagator (22) has a massless pole in the H channel corresponding to the Nambu-Goldstone boson.

For the purpose of clarifying the overall properties of collective excitations, it is instructive to investigate the spectral function, which is defined as

$$\rho(\omega, \vec{q}) = -\frac{1}{\pi} \text{Im} \mathbf{D}^R(\omega, \vec{q}). \quad (23)$$

In the subsequent sections we will calculate the dimensionless spectral functions in the H and vector channels:

$$\rho_H = \frac{6}{G} [\rho]_{HH}, \quad \rho_V = \frac{1}{G_V} [\rho]_{VV}, \quad (24)$$

where $[\rho]_{HH}$ is the H - H component of the 2×2 spectral matrix ρ and $[\rho]_{VV}$ is the V - V component. We will then identify the poles of the propagator in the complex energy plane that characterize the spectral shape.

IV. ZERO TEMPERATURE RESULTS

In this section, we analyze the spectral functions at zero temperature. We clarify the properties of H phonons in the CFL phase and of zero sound in the normal and CFL phases.

A. Phonon in a superfluid

We start with an H phonon in the CFL phase. This mode, usually denoted as H , can be interpreted as the Anderson-Bogoliubov mode [29] as encountered in neutral superfluids such as superfluid ^3He and superfluid neutron matter. In this mode, fluctuations in the phase of the superfluid order parameter are coupled with baryon density. Consequently, this mode behaves as a longitudinal compression mode; at zero temperature, its velocity is equal to the velocity of first sound. In the BCS framework, this mode can be viewed as a coherent superposition of Cooper pair excitations with total momentum \vec{q} , and hence it does not break up phase coherence in the superfluid state. We remark that as far as excitations associated with baryon number are concerned, symmetric CFL quark matter behaves like a neutral superfluid even though each quark pair carries electric and color charge.

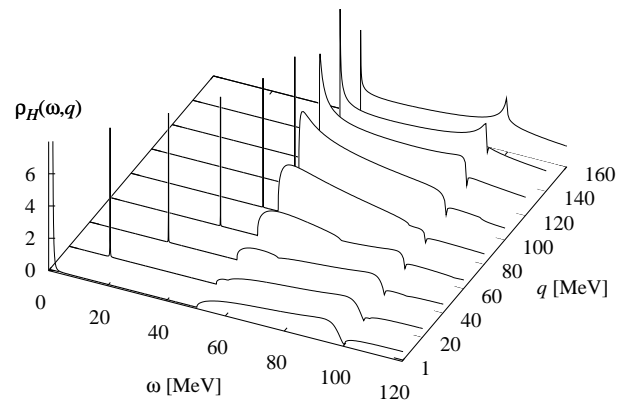


FIG. 3: Spectral function in the H channel at zero temperature.

As we have already seen, the H propagator has a massless pole. Correspondingly, the spectral function naturally has a δ -function peak. In the H channel the mixing effect makes only a little difference in the spectral function. As we shall see in the next subsection, however, it plays an important role in the vector channel.

From Fig. 3, we can clearly observe that a massless H mode appears as a δ -function peak (strictly speaking there is a small width coming from a finite regulator for numerical computations) and that the continuum starts at the threshold $\omega = 2\Delta$ above which individual pair excitations are kinematically allowed. The H mode always lies below the threshold; if lying above the threshold, it would be superseded by an excited Cooper pair, which eventually decay into two octet quark quasiparticles having an energy gap Δ . We remark that there appears a marked structure in the continuum around $\omega = 4\Delta$. This energy corresponds to a threshold above which individual pair excitations of singlet quarks are allowed to occur.

We can also observe that two spectral peaks near $\omega = 2\Delta$ and $\omega = 4\Delta$ are appreciable for $q \gtrsim 120$ MeV and that as the momentum q increases, they become sharper and sharper. This spectral enhancement of the continuum around $\omega = 2\Delta$ is analogous to the spectral enhancement as intensely argued in the chiral system of π and σ mesons in connection with chiral restoration [30, 31]. In the present case no phase transition occurs with increasing q , but it seems reasonable to consider that a superfluid behaves more like a normal fluid for larger q , which will be illustrated in the next subsection. In other words, the medium in which H propagates undergoes continuous changes from superfluid type to normal fluid type with increasing q .

This continuum structure characterized by the two distinct gaps for octet and singlet quarks is a unique feature of the CFL phase, which can be seen neither in superfluid ^3He nor in the 2SC phase, and provides useful information for identifying the CFL phase.

We remark that the two peaks near $\omega = 2\Delta$ and $\omega = 4\Delta$ do not move substantially until q exceeds $2\mu_\tau$. This is because the momenta of two quark quasiparticles, p

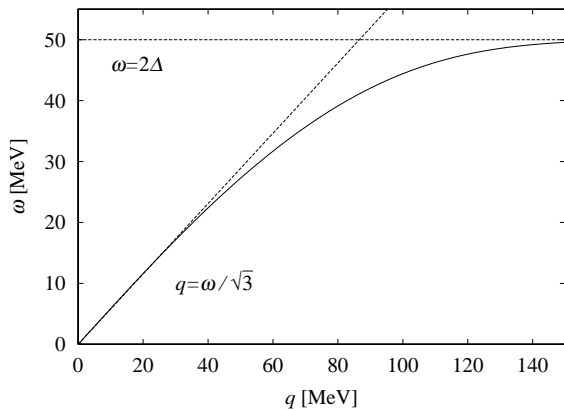


FIG. 4: The energy dispersion relation of H as a function of q at zero temperature.

and $|\vec{p} + \vec{q}|$, can sit on the Fermi surface simultaneously as long as $q < 2\mu_r$. We have confirmed that the peaks move upward for $q > 2\mu_r$, although we will not present the results here.

Another important property that can be observed from Fig. 3 is the excitation energy of H as a function of q , i.e., the energy dispersion relation of H . The excitation energy of H is proportional to q at small q , and monotonically increases with q in such a way as to approach the threshold $\omega = 2\Delta$ asymptotically. This behavior is consistent with the QCD analysis performed by Zarembo in weak coupling [32]. For further clarity, we plot our numerical results for the energy dispersion relation in Fig. 4. In the numerical calculations of the energy of H , we have ignored corrections by the mixing effect, which are in fact small at low energies and vanish at $\omega = 0$. The dispersion relation shown in Fig. 4 thus fulfills $6/G - \Pi_H(\omega, q) = 0$.

The earlier analyses based on the chiral effective Lagrangian [33] are valid for ω and q much lower than 2Δ . The present NJL model calculation is expected to reproduce the results from the low energy effective theories. As can be seen from Fig. 4, the speed of H is $v_H = 1/\sqrt{3}$, which is in agreement with the generally accepted value in the chiral effective Lagrangian approach. This is equal to the velocity of first sound, which is consistent with the fact that the restoring force of this mode is purely kinematic.

More technically, as shown in Ref. [34], the H velocity of $1/\sqrt{3}$ originates from the dimensionality (three spatial directions and one temporal direction). In the rest of this subsection we shall calculate the H decay constant, f_H , by following the line of the standard NJL calculation of f_π . Then, we shall consider how $v_H = 1/\sqrt{3}$ results from the ratio between the decay constants in the spatial direction, f_H^s , and in the temporal direction, f_H^t .

We can obtain f_H from the loop diagram shown in Fig. 5 as in the case of f_π in chiral dynamics. The dia-

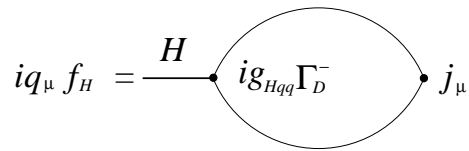


FIG. 5: Diagram contributing to f_H .

gram can be expressed as

$$\begin{aligned}
 iq_\mu f_H &= -\frac{1}{2} \int^T \frac{d^4 p}{(2\pi)^4} \text{tr} \frac{1}{2\sqrt{6}} \Gamma_V^\mu S(p_0 + q_0, \vec{p} + \vec{q}) ig_{Hqq} \Gamma_D^- S(p_0, \vec{p}), \\
 &= -\frac{1}{2} \int^T \frac{d^4 p}{(2\pi)^4} \text{tr} \frac{1}{2\sqrt{6}} \Gamma_V^\mu S(p_0 + q_0, \vec{p} + \vec{q}) ig_{Hqq} \Gamma_D^- S(p_0, \vec{p}),
 \end{aligned} \tag{25}$$

where the factor $1/2$ allows for the Nambu-Gor'kov counting, and the normalization factor $1/2\sqrt{6}$ in front of Γ_V^μ is determined so as to satisfy the proper current algebra. The H -quark coupling constant, g_{Hqq} , can be derived from the residue of the H propagator; the expression for g_{Hqq} is listed in Appendix A. Then, we find $f_H = (-1/\sqrt{6})\Delta g_{Hqq}^{-1}$. [The sign of f_H is irrelevant to observables because only its square, f_H^2 , appears in low energy effective theories [33].] After all we obtain the Goldberger-Treiman relation for quarks in the CFL phase,

$$(f_H \cdot g_{Hqq})^2 = \frac{1}{6} |\Delta|^2, \tag{26}$$

which was also derived in Ref. [34] from QCD in weak coupling. We note that g_{Hqq} remains finite and thus f_H vanishes in the limit $\Delta \rightarrow 0$ as it should.

When q^μ is infinitesimal and the temperature is much lower than the quark chemical potential, it is sufficient to limit our deliberation here to the particle part of the quark propagators in Eq. (25). Then, one can show that the integrand of Eq. (25) is proportional to q_0 in the limit, $\vec{q} = 0$ and $q_0 \simeq 0$, relevant for f_H^t , while this q_0 is replaced by $(\hat{p} \cdot \vec{q}) \hat{p}_i$ in the limit, $q_0 = 0$ and $q_i \simeq 0$, relevant for f_H^s . By noting the three-dimensional rotational symmetry, one can rewrite $\int d^3 p (\hat{p} \cdot \vec{q}) \hat{p}_i \dots$ as $(q_i/3) \int d^3 p \dots$. Consequently, the ratio f_H^s/f_H^t amounts to $g_{Hqq}^s/3g_{Hqq}^t$. By using this result, the relation $v_H^2 = (f_H^s/f_H^t)^2$ from the chiral effective Lagrangian, and the Goldberger-Treiman relation (26), we finally obtain

$$v_H^2 = \frac{1}{3}. \tag{27}$$

From the derivation of this result, it is clear that $1/3$ comes from the spatial dimensionality.

Let us next derive the expression for f_H in the NJL model. Using the Goldberger-Treiman relation (26) and the approximate zero-temperature expression (A8) for g_{Hqq}^t as derived in Appendix A, we can express the temporal decay constant at zero temperature as

$$(f_H^t)^2 \simeq \frac{3\mu_r^2}{8\pi^2}. \tag{28}$$

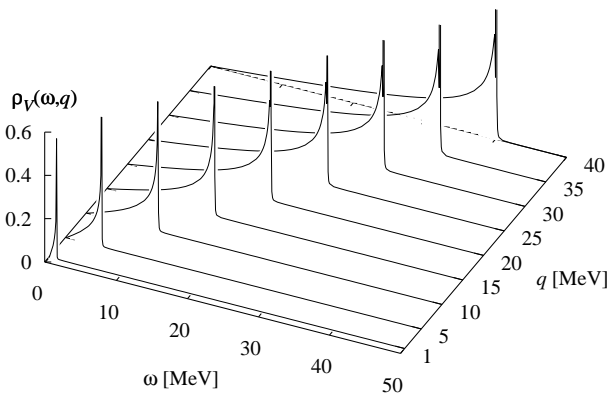


FIG. 6: Spectral function in the vector channel, calculated in the normal phase at zero temperature.

This result is the same as the one derived from QCD in weak coupling [33]. Here we emphasize that the mean-field quark propagator in the NJL model takes the same form as that in QCD in weak coupling. As long as diagrams composed of quarks are concerned, therefore, the NJL model and QCD yield essentially the same results within the mean-field approximation. This fact can explain why the NJL model calculations of f_π for CFL pions have been found to be close to the QCD results in Refs. [35, 36]. We remark that the same kind of agreement between the mean-field NJL and QCD calculations can be also found in the parameters characterizing the Ginzburg-Landau free energy [24].

The results for f_H and v_H obtained in this subsection imply that the NJL model calculations should encompass the results from chiral effective Lagrangian approach and even the QCD results in the mean-field approximation.

B. Zero sound

We turn to the analysis of the spectral function in the vector channel at zero temperature. There are two important features to be clarified in this subsection: the appearance of zero sound and the mixing effect between the H and vector channels. Zero sound is distinct from the H mode in the sense that it coherently involves a number of particle-hole excitations rather than pair excitations. We first articulate how zero sound emerges in the vector channel in a normal fluid of quark matter. We then consider zero sound in the CFL phase where the mixing effect plays an important role.

1. In the normal phase

In a normal fluid, where $\Delta = 0$ and the baryon number is conserved, no mixing between the H and vector channels arises, and we can deal with the vector channel alone. Our primary results are illustrated in Fig. 6

where the spectral function in the vector channel is plotted. In calculating the vector spectral function in the normal phase, we have fixed all the parameters at the values adopted in the previous section except Δ , which is set to be zero. We can observe from the figure that the continuum ranges $0 \leq \omega \leq q$ and that an undamped mode (zero sound) stands in the vicinity of the continuum, although it is rather hard to see in the plot that the δ -function peak is away from the continuum.

The continuum in the spectral function stems from individual excitations of quark particle-hole pairs. The continuum corresponds to the space-like region $\omega < q$. In the present NJL model, the energy of a quasiparticle of momentum \vec{k} is k as in the case of a massless free quark gas. For a real pair of a particle of momentum \vec{k}_1 and a hole of momentum \vec{k}_2 , therefore, we can calculate the excitation energy as $\omega = (k_1 - \mu_r) + (\mu_r - k_2) \leq q$, where $\vec{q} = \vec{k}_2 - \vec{k}_1$ is the momentum of the pair.

If zero sound lies in the continuum, it would suffer Landau damping. In this case, zero sound would be absorbed by a quasiparticle with momentum below the Fermi surface, which subsequently would be scattered into a state above the Fermi surface. This process corresponds to the decay of zero sound into a real particle-hole pair, which is kinematically allowed only when $\omega < q$. As we shall show explicitly, however, the calculated dispersion relation lies above the continuum.

We now proceed to determine the velocity of zero sound by following a line of the conventional field-theoretical argument [37]. Let us focus on the expression for Π_V , which is given by Eq. (A3) in the limit of $\Delta \rightarrow 0$. At zero temperature the quasiparticle distribution function vanishes. The dominant term that remains in Π_V is then

$$\begin{aligned} \Pi_V(\omega, \vec{q}) \simeq & 18 \int \frac{d^3 p}{(2\pi)^3} \left[\Theta(p - \mu_r) \Theta(\mu_r - |\vec{p} + \vec{q}|) \right. \\ & \left. + \Theta(\mu_r - p) \Theta(|\vec{p} + \vec{q}| - \mu_r) \right] \frac{||\vec{p} + \vec{q}| - \mu_r| + |p - \mu_r|}{\left(||\vec{p} + \vec{q}| - \mu_r| + |p - \mu_r| \right)^2 - \omega^2}. \end{aligned} \quad (29)$$

Here Θ denotes the Heviside's step function. The first (second) term in the square brackets corresponds to a virtual excitation of a particle (hole) with momentum \vec{p} and a hole (particle) with momentum $\vec{p} + \vec{q}$. Because of these terms, the dominant contribution to Π_V comes from a regime that satisfies $p \simeq \mu_r$ and $\omega, q \ll \mu_r$. We can thus use the approximation, $|\vec{p} + \vec{q}| \simeq p + \hat{p} \cdot \vec{q}$. Eventually, Π_V can be estimated as

$$\Pi_V(\omega, \vec{q}) \simeq \frac{18\mu_r^2 q^2}{(2\pi)^3} \int d\Omega \frac{(\vec{n} \cdot \vec{q})^2}{q^2 (\vec{n} \cdot \vec{q})^2 - \omega^2}, \quad (30)$$

where $\int d\Omega = 2\pi \int_{-1}^1 d\cos\theta$ and $\vec{n} \cdot \hat{q} = \cos\theta$.

By defining the zero sound velocity as $v_0 = \omega/q$ and using Eq. (30), we can rewrite the zero sound dispersion

relation, $1/G_V + \Pi_V(\omega, q) = 0$, as

$$\frac{v_0}{2} \ln \left| \frac{v_0 + 1}{v_0 - 1} \right| - 1 = \frac{1}{G_V} \cdot \frac{\pi^2}{9\mu_r^2}. \quad (31)$$

This agrees with the conventional form of the nonrelativistic zero sound equation (see Eq. (2.26) of Ref. [37]). Since the right side of Eq. (31) is 2.304 for our parameter choice, we obtain $v_0 = 1.0028$ as a solution to Eq. (31). Our numerical results for $q = 40$ MeV, on the other hand, has a δ -function peak at $\omega = 40.11$ MeV, from which we can derive the speed as $v_0 = 40.11/40 = 1.0028$. This value is in excellent agreement with the analytic estimate.

It is to be noted that the velocity of zero sound is slightly larger than unity. This uncausal behavior is due to our negligence of the longitudinal spatial components of the bubble diagrams in the vector channel, which contain a term proportional to the cut-off squared Λ^2 . We have confirmed that our calculations, if including the longitudinal spatial components, would give rise to zero sound of velocity below unity, which is damped in the continuum. However, it is more important to note that the Fermi velocity is unity since our model ignores the quark wave-function renormalization. Undamped zero sound, if present, would thus be automatically superluminal. In the high density limit of QCD in which one-gluon exchange dominates the quark-quark interactions, on the other hand, the bubble diagram in the vector channel yields a continuum in the spectral function at $\omega < v_F q < q$, where v_F is the Fermi velocity, and an undamped zero sound mode of velocity less than unity but larger than v_F [19]. Our calculations, therefore, are successful in reproducing the weak coupling behavior of zero sound predicted from QCD, except for the slightly superluminal velocity of sound. We thus believe that our framework gives a sufficient basis in analyzing the properties of zero sound in the CFL phase, as will be discussed below.

2. In the CFL phase

Let us now examine zero sound and H -vector mixing in the CFL phase. We first present our numerical results for the spectral function in the vector channel and then discuss the underlying physics of the observed spectral suppression at small q and attenuation of zero sound.

We plot the spectral function in the vector channel in Fig. 7, which is to be compared with Fig. 6. The spectral functions displayed in Figs. 6 and 7 are markedly different in two respects: In the CFL phase a δ -function peak corresponding to an H phonon in the space-like ($\omega < q$) region appears, and a peak corresponding to zero sound, located at $\omega \simeq 78$ MeV for $q = 60$ MeV, at $\omega \simeq 94$ MeV for $q = 80$ MeV, and at $\omega \simeq 111$ MeV for $q = 100$ MeV, has a width in the continuum that extends above $\omega = 2\Delta$. As a result of the H -vector mixing, the H phonon peak and continuum similar to the ones in the H channel as

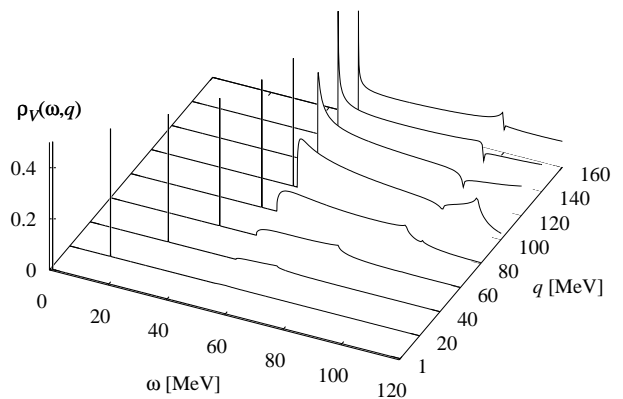


FIG. 7: Spectral function in the vector channel, calculated in the CFL phase at zero temperature.

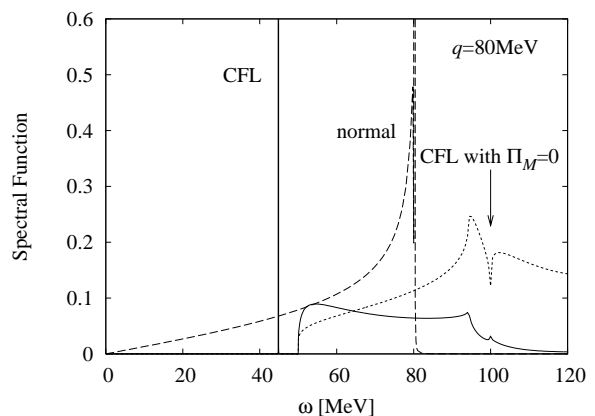


FIG. 8: Spectral functions for $q = 80$ MeV in the vector channel, calculated in the normal phase (dashed line), in the CFL phase without mixing (dotted line), and in the CFL phase with mixing (solid line). The zero sound peak at $\omega \simeq 80$ MeV in the normal phase shifts to $\omega \simeq 94$ MeV with an attenuation width in the CFL phase.

shown in Fig. 3 do appear in the vector channel, but have a vanishingly small spectral weight at $q \simeq 0$. On the other hand, the observed width of the zero sound peak indicates the attenuation of zero sound. In order to see how the attenuation and the mixing effect affect the spectral function, we plot in Fig. 8 three spectral functions calculated in the normal phase, in the CFL phase by ignoring the mixing effect, and in the CFL phase by including the mixing effect.

First, we discuss the strong spectral suppression in the vector channel at $q \simeq 0$ and the underlying mixing effect between the H and vector channels. In the long wavelength limit $q = 0$, a clear distinction between particle and hole excitations is lost in the superfluid medium, and only the H (particle-particle) channel contributes to the spectral weight. For q far larger than Δ , on the other hand, the medium behaves more like a normal fluid rather than a superfluid, and the vector (particle-hole) channel exhibits a similar spectral function to that in the normal

phase.

We can explicitly show the spectral suppression by noting that the bubble diagrams in the limit $q \rightarrow 0$ satisfy the relations,

$$\begin{aligned}\Pi_H(\omega, 0) &= \Pi_H(0, 0) + \frac{\omega^2}{4\Delta^2}\Pi_V(\omega, 0) \\ &= \frac{6}{G} + \frac{\omega^2}{4\Delta^2}\Pi_V(\omega, 0),\end{aligned}\quad (32)$$

$$\Pi_M(\omega, 0) = -\frac{i\omega}{2\Delta}\Pi_V(\omega, 0). \quad (33)$$

As a result of these relations, the vector component of the propagator matrix (22) reduces to $-G_V$, which is exactly the tree-level value (the cross diagram in Fig. 2). This indicates that the vector channel no longer contains the quark loops responsible for collective and individual excitations, leading to a vanishing spectral function. In other words, any excitations with small momenta in the vector channel tend to be absorbed into the H channel in the superfluid medium. As q becomes larger, the vector spectral function grows in the medium in which particle and hole excitations are no longer indistinguishable, leading to a zero sound peak.

This difference in the vector channel at small q between the normal and CFL phases could serve as a possible diagnosis of superfluidity of quark matter if the spectral function in the vector channel could be measured in the lattice QCD simulation. Quark matter could be considered to be in the normal phase when zero sound is found at small q , while in the superfluid phase when strong spectral suppression or weak mixture with an H phonon is observed. One could distinguish between zero sound and an H phonon from the fact that the H phonon velocity is smaller than the zero sound velocity by a factor of $\sim 1/\sqrt{3}$ except for Fermi-liquid corrections. In fact, zero sound has been found in the lattice simulation based on a QCD-like model [16]. If the simulation involves a superfluid phase, the vector channel measurement would provide a clear signature of superfluidity.

We next discuss the attenuation of zero sound in the continuum. In order to extract detailed information on zero sound, we search for a pole of the vector propagator in the complex energy plane, which is responsible for a weak peak in the spectral function in the vector channel. For simplicity we ignore the H -vector mixing and the antiparticle contribution in locating the complex pole position. This kind of pole search has been performed in the context of chiral restoration in a hot and dense medium [31] and of a phase transition from the normal to the 2SC phase [2]. Appendix B is devoted to exhibiting how to perform the analytic continuation into the second Riemann sheet where the attenuated mode would be found.

In Figs. 9 and 10 we plot the pole position, ω , as a function of q . We can observe from Fig. 9 that the real part of ω almost linearly increases with q once q becomes larger than $\sim 2\Delta$. Since there is no quark excitation at

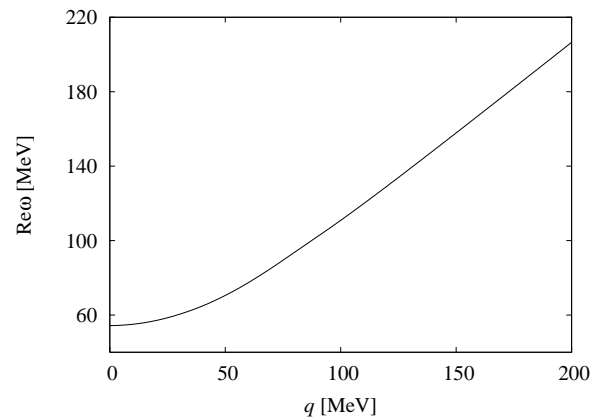


FIG. 9: The real part of the zero sound pole in the CFL phase at zero temperature.

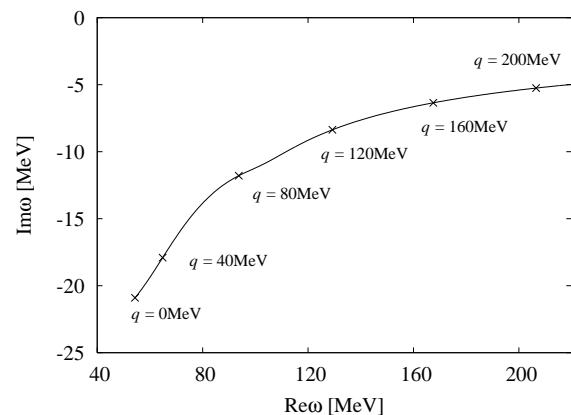


FIG. 10: The pole position of zero sound in the CFL phase at zero temperature. The curve is slightly distorted when it passes through the threshold energy $\text{Re}\omega = 100$ MeV for individual pair excitations of singlet quarks.

low ω due to a nonzero pairing gap, zero sound, a coherent superposition of particle-hole pairs, can only emerge in the continuum where quasiparticle modes are allowed to excite. This explains why the energy of zero sound has a gap and stays slightly larger than 2Δ for $q \rightarrow 0$.

Figure 10 illustrates how the pole moves in the complex energy plane with increasing q . The width of zero sound attenuation decreases with q . This attenuation occurs in the superfluid medium in which zero sound is absorbed by a Cooper pair, which subsequently breaks up into two quasiparticles. Consequently, the decrease in the width with increasing q is consistent with the tendency that the medium behaves more like a normal fluid for elementary excitations with larger q . Recall that zero sound in the normal phase is undamped in the present analysis.

We conclude this section by summarizing the zero-temperature results for an H phonon and zero sound in the CFL phase. H phonons are only low-lying longitudinal excitations and survive as long as $\omega < 2\Delta$, while zero sound manifests itself as an attenuated mode for $\omega > 2\Delta$.

The former is consistent with the earlier results from low energy effective theories. The latter is the point that we first clarified in the context of superfluid quark matter. The presence of the phase and zero sound modes in different regimes of ω can also be seen in superfluid ^3He [18]. We also discovered a strong spectral suppression in the vector channel at small q . We remark in passing that all these properties of the CFL state are robust even if the longitudinal spatial components of the bubble diagrams in the vector channel are taken into account.

V. FINITE TEMPERATURE RESULTS

In this section we examine thermal effects on collective excitations in the collisionless limit. The collisions between quasiparticles, which are expected to play a role in modifying the properties of the collective modes at finite temperatures, will be addressed in our future study. At finite temperatures, as we shall see, the H modes are Landau damped by thermally excited quark quasiparticles, while the behavior of zero sound is essentially the same as that obtained at zero temperature. Throughout this section we limit ourselves to the case at $T = 0.8T_c = 14.52 \text{ MeV}$, which is high enough for us to perceive the temperature effect in the H channel, while not being in the immediate vicinity of the critical point. At this temperature, the pairing gap and the effective chemical potential can be calculated as $\Delta = 16.4 \text{ MeV}$ and $\mu_r = 435.3 \text{ MeV}$. The temperature dependence of μ_r turns out to be tiny; even just above T_c , μ_r is greater than the zero temperature value only by 2%.

We first consider zero sound, which, at zero temperature, appears as a low-lying mode in the normal phase and as an attenuated mode above 2Δ in the CFL phase, as we have seen in Sec. IV B. The behavior of zero sound at $T = 0.8T_c$ and at $T = 0$ is almost indistinguishable. This is because $T = 0.8T_c = 14.52 \text{ MeV}$ is *low* compared with the Fermi temperature corresponding to the quark chemical potential $\sim 500 \text{ MeV}$. In the normal phase, unless the temperature is considerably higher than T_c , no drastic change occurs in the behavior of zero sound from that shown in Fig. 6.

In contrast to the case of zero sound, H modes in the CFL phase are damped only at nonzero temperatures. In the case in which thermally excited quark quasiparticles are present, the H modes suffer Landau damping. This process can be viewed as the upscattering of a quasiparticle by absorbing a H phonon, which is characterized by the nonvanishing factor $[n_F^- - n_F^{-\prime}]$ in Eq. (A2). The similar damping process of the phase modes has been considered in the context of neutral BCS superfluids [38]. The Landau damping of the H modes can be observed from Fig. 11 in which the spectral function in the H channel is plotted at $T = 0.8T_c$. We find that the H modes have a finite decay width in contrast to the zero temperature case as shown in Fig. 3. The threshold for pair excitations is located at $\omega = 2\Delta = 32.8 \text{ MeV}$. We also note that as a

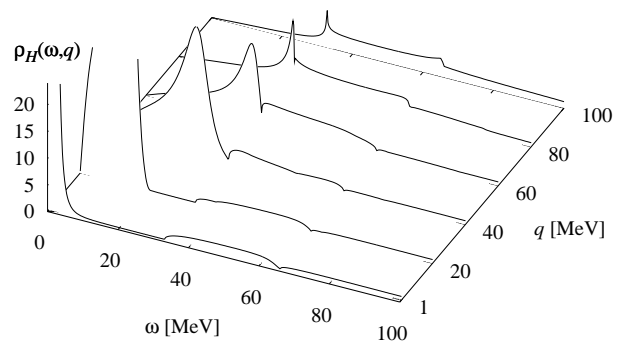


FIG. 11: Spectral function in the H channel, calculated in the CFL phase at $T = 0.8T_c$.

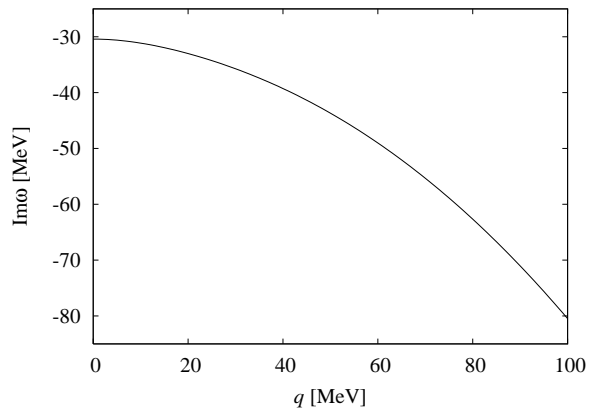


FIG. 12: The pole position of the diffusive mode responsible for the Landau damping in the CFL phase at $T = 0.8T_c$.

result of the Landau damping, the spectral function has a continuum below the H peak.

Detailed analysis shows that the velocity of the H mode at $T = 0.8T_c$ is $v_H = 0.554$ which is slightly smaller than $1/\sqrt{3}$. This is because the superfluid part rather than the whole system participates in the phase fluctuations.

Now, we briefly discuss the possible relevance of our results to the transport properties in the CFL phase. In the H channel, by setting $\Pi_M = 0$ for simplicity, we can find a pole on the imaginary axis in the complex energy plane. This pure imaginary pole corresponds to a diffusive mode that does not propagate at all. We identify this imaginary pole as responsible for the low-lying continuum due to the Landau damping.

In Fig. 12 we plot the pole position as a function of the momentum q . The result can be parametrized as $\text{Im} \omega = -30.9 - 5.11 \times 10^{-3} q^2 \text{ [MeV]}$. This result suggests that H modes in CFL quark matter suffer diffusion with the diffusion constant $5.11 \times 10^{-3} \text{ MeV}^{-1}$ in addition to absorption. This diffusion coefficient arises even in the collisionless limit, but has to be modified by collisions between quasiparticles, which are more relevant at higher temperatures.

Although description of collective modes in the hydro-

dynamic regime is beyond the scope of the present paper, we shall comment on what is expected in the hydrodynamic regime. In the normal phase, as in a normal liquid ^3He , zero sound in the collisionless regime should continuously transform to first sound in the hydrodynamic regime. In the superfluid medium, as discussed in Ref. [39] and also pointed out in Ref. [26], the mode corresponding to phase oscillations in the collisionless regime should change into second sound in the hydrodynamic regime. It would be an interesting future problem to describe such continuous transitions in the nature of sound modes within the framework of kinetic theory.

VI. CONCLUDING REMARKS

In this paper we have studied the longitudinal spectral functions in the H and vector channels in a superfluid of CFL quark matter. We have elucidated the zero-temperature properties of the vector channel: the strong spectral suppression at small momenta due to the H -vector mixing and the zero sound attenuation above the energy threshold for pair excitations. The important implication of these results is that the spectral function in the vector channel is sensitive to the state of quark matter. If lattice QCD simulation at finite density is feasible in the future, the vector channel measurements could be of great use for identifying superfluidity of quark matter.

Extension of the present analysis to the case of nonzero quark masses is desirable for the description of elementary excitations in realistic situations. In this case, as discussed in Sec. II, the possible coupling of phase and baryon density fluctuations with electric and/or color charge density fluctuations could change the properties of the longitudinal collective excitations drastically. In the presence of gapless quark modes as in the gapless CFL phase [25], the continuum of the quark excitations and hence the attenuation of the collective modes would be enhanced.

In the present analysis we have utilized the NJL model for quark matter. The NJL model description turns out to reproduce the results for H phonons known from low-energy effective theories and even from QCD in the mean-

field approximation. In the collisionless regime, however, the longitudinal spectral functions remain to be clarified from QCD even in weak coupling. Furthermore, collective modes in the CFL phase have yet to be examined in the hydrodynamic regime. It would be instructive to describe low-lying excitations of CFL quark matter in both regimes by using a relativistic version of the Landau theory of Fermi liquids [19], which effectively encompasses the NJL model.

Acknowledgments

We are grateful to G. Baym and T. Hatsuda for valuable comments on these and related subjects. K. F. thanks M. Forbes, C. Kouvaris, K. Rajagopal, and D. T. Son for discussions. This work was partially supported by the Japan Society for the Promotion of Science for Young Scientists and by the U.S. Department of Energy (D.O.E.) under cooperative research agreement #DF-FC02-94ER40818.

APPENDIX A: EVALUATION OF THE BUBBLE DIAGRAMS

In this appendix, we present the explicit expressions for the polarization functions in the H , vector, and mixed channels. We also provide the calculation of g_{Hqq} which is a derivative of the polarization with respect to either energy or momentum. Since the quark propagator is divided into the particle part and the antiparticle part as displayed in Eq. (7), the bubble diagram in the l channel ($l = H, V, M$) can be divided into four parts as

$$\Pi_l = \Pi_l^{\text{pp}} + \Pi_l^{\text{aa}} + \Pi_l^{\text{pa}} + \Pi_l^{\text{ap}}, \quad (\text{A1})$$

where the superscript ‘‘p’’ and ‘‘a’’ denote the particle and antiparticle parts of the quark propagator, respectively.

We begin with the expression for the polarization Π_H in the H channel. The particle-particle part can be written as

$$\begin{aligned} \Pi_H^{\text{pp}}(\omega, \vec{q}) &= 2 \int^\Lambda \frac{d^3p}{(2\pi)^3} [1 + \widehat{p} \cdot (\widehat{p} + \vec{q})] \frac{1}{\epsilon_\Delta^- \epsilon_\Delta'^-} \\ &\times \left\{ \left[\epsilon_\Delta^- \epsilon_\Delta'^- + (p - \mu_r)(|\vec{p} + \vec{q}| - \mu_r) + \Delta^2 \right] \left(\frac{1}{\omega + \epsilon_\Delta^- + \epsilon_\Delta'^-} - \frac{1}{\omega - \epsilon_\Delta^- - \epsilon_\Delta'^-} \right) [1 - n_{\text{F}}^- - n_{\text{F}}'^-] \right. \\ &\quad \left. + \left[\epsilon_\Delta^- \epsilon_\Delta'^- - (p - \mu_r)(|\vec{p} + \vec{q}| - \mu_r) - \Delta^2 \right] \left(\frac{1}{\omega - \epsilon_\Delta^- + \epsilon_\Delta'^-} - \frac{1}{\omega + \epsilon_\Delta^- - \epsilon_\Delta'^-} \right) [n_{\text{F}}^- - n_{\text{F}}'^-] \right\} \\ &\quad + \frac{1}{2}(\text{same with } \Delta \rightarrow 2\Delta), \end{aligned} \quad (\text{A2})$$

where we have used the notations for the quark excitation energies, $\epsilon_{\Delta}^{-} = \epsilon_{\Delta}^{-}(\vec{p})$ and $\epsilon_{\Delta}^{-'} = \epsilon_{\Delta}^{-}(\vec{p} + \vec{q})$, and for the Dirac-Fermi distribution functions, $n_{\text{F}}^{-} = [e^{\epsilon_{\Delta}^{-}/T} + 1]^{-1}$ and $n_{\text{F}}^{-'} = [e^{\epsilon_{\Delta}^{-'}/T} + 1]^{-1}$. The antiparticle-antiparticle part, Π_H^{aa} , can be readily obtained from expression (A2) by replacing μ_r by $-\mu_r$. [Note that by this replacement ϵ^{-} is replaced by ϵ^{+} .] One can obtain the expression for the particle-antiparticle part Π_H^{pa} by replacing, in Eq. (A2), $(p - \mu_r)$ by $-(p + \mu_r)$, ϵ_{Δ}^{-} by ϵ_{Δ}^{+} , n_{F}^{-} by n_{F}^{+} , and $1 + \widehat{p} \cdot (\widehat{p} + \widehat{q})$ by $1 - \widehat{p} \cdot (\widehat{p} + \widehat{q})$. The antiparticle-particle part, Π_H^{ap} , likewise obtains.

The particle-particle part of the bubble diagram in the vector channel reads

$$\begin{aligned} \Pi_V^{\text{pp}}(\omega, \vec{q}) &= 2 \int^{\Lambda} \frac{d^3 p}{(2\pi)^3} [1 + \widehat{p} \cdot (\widehat{p} + \widehat{q})] \frac{1}{\epsilon_{\Delta}^{-} \epsilon_{\Delta}^{-'}} \\ &\times \left\{ \left[\epsilon_{\Delta}^{-} \epsilon_{\Delta}^{-'} - (p - \mu_r)(|\vec{p} + \vec{q}| - \mu_r) + \Delta^2 \right] \left(\frac{1}{\omega + \epsilon_{\Delta}^{-} + \epsilon_{\Delta}^{-'}} - \frac{1}{\omega - \epsilon_{\Delta}^{-} - \epsilon_{\Delta}^{-'}} \right) [1 - n_{\text{F}}^{-} - n_{\text{F}}^{-'}] \right. \\ &\quad \left. + \left[\epsilon_{\Delta}^{-} \epsilon_{\Delta}^{-'} + (p - \mu_r)(|\vec{p} + \vec{q}| - \mu_r) - \Delta^2 \right] \left(\frac{1}{\omega - \epsilon_{\Delta}^{-} + \epsilon_{\Delta}^{-'}} - \frac{1}{\omega + \epsilon_{\Delta}^{-} - \epsilon_{\Delta}^{-'}} \right) [n_{\text{F}}^{-} - n_{\text{F}}^{-'}] \right\} \\ &\quad + \frac{1}{8} (\text{same with } \Delta \rightarrow 2\Delta). \end{aligned} \quad (\text{A3})$$

This is the same as Π_H^{pp} except for the sign in front of the factor $(p - \mu_r)(|\vec{p} + \vec{q}| - \mu_r)$ and the coefficient affixed to the singlet contribution. This change in the sign can be intuitively understood once the limit of $\Delta \rightarrow 0$ is taken. In this limit, as discussed in Sec. IV B, the integrand is nonzero only when one of the factors $(p - \mu_r)$ and $(|\vec{p} + \vec{q}| - \mu_r)$ is positive and the other is negative. This situation corresponds to a simultaneous excitation of a quark particle above the Fermi surface and a quark hole below the Fermi surface, rather than pair excitations which play a role in Π_H^{pp} . In the presence of the energy gap Δ , the clear distinction between particles and holes is lost since the quasiparticle state appears as a linear superposition of a particle state and a hole state. The other parts, Π_V^{aa} , Π_V^{pa} , and Π_V^{ap} , obtain in the same way as in the H channel.

We remark that Π_V^{pp} is almost independent of the cut-off Λ because the momentum integration around the Fermi surface contributes dominantly to Π_V^{pp} . For suffi-

ciently large p to satisfy $|\vec{p} + \vec{q}| > \mu_r$, a hole is not allowed to excite at zero temperature, so that the momentum integration has a natural cut-off. In contrast, Π_V^{pa} has an appreciable dependence on Λ since an antiparticle can arise at arbitrary \vec{p} . This cut-off dependent contribution is, however, suppressed by a factor of q^2/p^2 because of the orthogonality between the positive and negative energy states, i.e., $\text{tr} \Lambda_{p+q}^{\pm} \Lambda_p^{\mp} = 1 - \widehat{p} \cdot (\widehat{p} + \widehat{q})$. If we take account of the spatial component of the polarization, Π_V^{33} , for instance, a particular choice of the polarizing direction leads to breaking of the orthogonality. As a result the particle-antiparticle contribution of Π_V^{33} has a term proportional to the cut-off squared Λ^2 , and hence the cut-off dependence of Π_V^{33} is not well controllable in contrast to the case of Π_V^{00} considered here.

We turn to the expression for the polarization Π_M in the mixed channel. The particle-particle part reads

$$\begin{aligned} \Pi_M^{\text{pp}}(\omega, \vec{q}) &= -2i\Delta\omega \int^{\Lambda} \frac{d^3 p}{(2\pi)^3} [1 + \widehat{p} \cdot (\widehat{p} + \widehat{q})] \frac{1}{\epsilon_{\Delta}^{-} \epsilon_{\Delta}^{-'}} \left\{ \left(\frac{1}{\omega + \epsilon_{\Delta}^{-} + \epsilon_{\Delta}^{-'}} - \frac{1}{\omega - \epsilon_{\Delta}^{-} - \epsilon_{\Delta}^{-'}} \right) [1 - n_{\text{F}}^{-} - n_{\text{F}}^{-'}] \right. \\ &\quad \left. - \left(\frac{1}{\omega - \epsilon_{\Delta}^{-} + \epsilon_{\Delta}^{-'}} - \frac{1}{\omega + \epsilon_{\Delta}^{-} - \epsilon_{\Delta}^{-'}} \right) [n_{\text{F}}^{-} - n_{\text{F}}^{-'}] \right\} + \frac{1}{4} (\text{same with } \Delta \rightarrow 2\Delta), \end{aligned} \quad (\text{A4})$$

and Π_M^{aa} , Π_M^{pa} , and Π_M^{ap} obtain in the same way as in the H channel.

From the expression for Π_H obtained above, we can calculate the coupling constant between H and quarks, which is determined by the residue of the H propagator

as

$$g_{Hqq}^2 = \left[\frac{\partial \Pi_H}{\partial q^{\mu} q_{\mu}} \right]_{q^{\mu} q_{\mu} = m_H^2 = 0}^{-1}, \quad (\text{A5})$$

where m_H is the H mass. We note that since $m_H = 0$,

the mixed part Π_M does not contribute to g_{Hqq} . Since Lorentz symmetry is broken in a many particle system, the derivatives in the temporal and spatial directions lead to different results, which in turn yield the velocity of the H mode smaller than unity.

We can write down the derivative in the temporal direction as

$$(g_{Hqq}^t)^{-2} = \left. \frac{\partial \Pi_H^{\text{pp}}(\omega, 0)}{\partial \omega^2} \right|_{\omega=0} \quad (\text{A6})$$

$$= 2 \int^\Lambda \frac{d^3 p}{(2\pi)^3} \frac{1 - 2n_F}{(\epsilon_\Delta^-)^3} + \frac{1}{2} (\text{same with } \Delta \rightarrow 2\Delta)$$

for the particle-particle part. Here we note that $\Pi_H^{\text{ap}}(\omega, 0) = 0$ and that Π_H^{aa} is suppressed compared with Π_H^{pp} since ϵ_Δ^- in Π_H^{pp} is replaced by ϵ_Δ^+ in Π_H^{aa} . At zero temperature we can estimate the integral in Eq. (A6), by assuming that it is dominated by momenta close to the Fermi surface, as

$$\int \frac{d^3 p}{(2\pi)^3} \frac{1}{(\epsilon_\Delta^-)^3} \simeq \frac{\mu_r^2}{2\pi^2} \int_{-\infty}^{\infty} \frac{dp}{(p^2 + \Delta^2)^{3/2}} = \frac{\mu_r^2}{\pi^2 \Delta^2}. \quad (\text{A7})$$

We thus obtain the temporal H -quark coupling constant at zero temperature as

$$(g_{Hqq}^t)^{-2} = \frac{9\mu_r^2}{4\pi^2 \Delta^2}. \quad (\text{A8})$$

We next estimate from Eq. (A5) the spatial H -quark coupling constant at zero temperature. The differentiation in the spatial direction involved in this estimate is more complicated than that in the temporal direction. By expanding the integrand of $\Pi_H^{\text{pp}}(0, \vec{q})$ with respect to q , we find that the term proportional to q^2 is smaller than the term proportional to $(\hat{p} \cdot \hat{q})^2$ by a factor of Δ^2/μ_r^2 . We thus neglect the former term. Then, the integrand of $\partial \Pi_H^{\text{pp}}(0, \vec{q})/\partial q^2$ reduces to

$$\frac{\Delta^4 + (\epsilon_\Delta^-)^2(\mu_r^2 - 3\mu_r p + 3p^2) + \Delta^2(\mu_r^2 - 2\mu_r p - 2p^2)}{(\epsilon_\Delta^-)^5}. \quad (\text{A9})$$

Note that the integral with respect to p is dominated by momenta close to the Fermi surface. We can thus simplify the integrand by dropping the Δ^4 term and by setting $p = \mu_r$ in the numerator as

$$\simeq \frac{\mu_r^2[(\epsilon_\Delta^-)^2 - 3\Delta^2]}{(\epsilon_\Delta^-)^5}. \quad (\text{A10})$$

We finally obtain

$$(g_{Hqq}^s)^{-2} = - \left. \frac{\partial \Pi_H^{\text{pp}}(0, q)}{\partial q^2} \right|_{q=0} \quad (\text{A11})$$

$$= 2 \int^\Lambda \frac{d^3 p}{(2\pi)^3} \frac{(\hat{p} \cdot \hat{q})^2}{(\epsilon_\Delta^-)^3} = \frac{1}{3} (g_{Hqq}^t)^{-2},$$

where we have used the relation $\int dp (\epsilon_\Delta^-)^{-5} = (2/3\Delta^2) \int dp (\epsilon_\Delta^-)^{-3}$, and the factor $1/3$ originates from the average over three spatial directions.

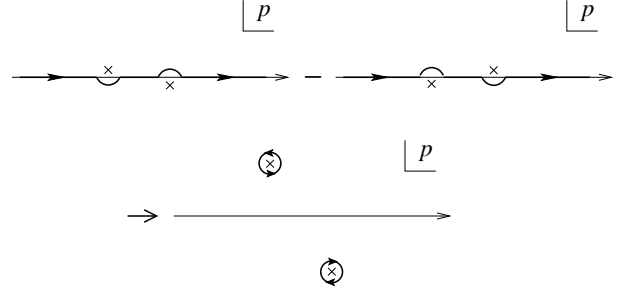


FIG. 13: Poles off the real axis in the complex p plane. We can perform the analytic continuation by picking up the positive residue of poles in the upper-half plane and the negative residue of poles in the lower-half plane.

APPENDIX B: ANALYTIC CONTINUATION TO THE SECOND RIEMANN SHEET

Here we explain how to perform the analytic continuation to the second Riemann sheet on which possible unstable states would have a pole. In the imaginary-time formalism of finite temperature field theory, the real-time retarded propagator, $\mathbf{D}^R(\omega, \vec{q})$, can be obtained by the analytic continuation, $\mathbf{D}^R(\omega, \vec{q}) = \mathbf{D}(q_0 = \omega + i0^+, \vec{q})$. When ω is larger than the threshold for single particle excitations, the propagator has a finite imaginary part, which leads to the spectral function having a continuum. Then, the propagator and hence the polarization $\mathbf{\Pi}(\omega, \vec{q})$ has a branch cut in the complex energy plane.

If we take $\mathbf{\Pi}(z = \zeta - i\eta, \vec{q})$ as an analytically continued function, this polarization in the limit of $\eta \rightarrow 0$ is not continuously connected to $\mathbf{\Pi}(\zeta + i0^+, \vec{q})$ in the physical sheet due to a branch cut in the continuum region. In order to remedy this situation, it is convenient to add the discontinuity,

$$\text{Disc}\mathbf{\Pi}(\omega, \vec{q}) = \mathbf{\Pi}(\omega + i0^+, \vec{q}) - \mathbf{\Pi}(\omega + i0^-, \vec{q}). \quad (\text{B1})$$

Once we know the analytic continuation of $\text{Disc}\mathbf{\Pi}(\omega, \vec{q})$, we can locate the pole in the second Riemann sheet by using $\mathbf{\Pi}(z, \vec{q}) + \text{Disc}\mathbf{\Pi}(z, \vec{q})$ as a properly analytically continued function.

In our calculation $\mathbf{\Pi}$ is not written as a closed expression, but, as listed in Appendix A, an expression involving the momentum integration with respect to p . For the energy $\omega + i0^+$, the integrand has in general several poles stemming from $1/(\omega - \epsilon_\Delta^- - \epsilon_\Delta'^-)$ and other similar terms in the complex p plane. These poles lie either above or below the real axis as shown in Fig. 13. Then, as is obvious from the figure, $\text{Disc}\mathbf{\Pi}$ is nothing but the contour integrals around the poles. If a pole is above (below) the real axis, the contour goes in the positive (negative) orientation. Straightforward generalization of this computational rule to the case of complex ω yields the analytic continuation. For complex $\omega = z$, poles are not necessarily distributed in the vicinity of the real axis. Then, we can calculate $\text{Disc}\mathbf{\Pi}(z, \vec{q})$ from the contour integrals around the poles as shown in the lower part of

Fig. 13.

-
- [1] For reviews, see K. Rajagopal and F. Wilczek, arXiv:hep-ph/0011333; M. G. Alford, Ann. Rev. Nucl. Part. Sci. **51**, 131 (2001) [arXiv:hep-ph/0102047]; G. Nardulli, Riv. Nuovo Cim. **25N3**, 1 (2002) [arXiv:hep-ph/0202037]; S. Reddy, Acta Phys. Polon. B **33**, 4101 (2002) [arXiv:nucl-th/0211045]; T. Schäfer, arXiv:hep-ph/0304281; M. Alford, Prog. Theor. Phys. Suppl. **153**, 1 (2004) [arXiv:nucl-th/0312007]. M. Huang, arXiv:hep-ph/0409167.
- [2] M. Kitazawa, T. Koide, T. Kunihiro, and Y. Nemoto, Phys. Rev. D **65**, 091504 (2002) [arXiv:nucl-th/0111022]; M. Iwasaki, K. Yamaguchi and O. Miyamura, Phys. Rev. D **66**, 094008 (2002) [arXiv:hep-ph/0112194].
- [3] G. W. Carter and S. Reddy, Phys. Rev. D **62**, 103002 (2000) [arXiv:hep-ph/0005228]; G. W. Carter, eConf **C010815**, 149 (2002) [arXiv:hep-ph/0111353].
- [4] D. Page, M. Prakash, J. M. Lattimer, and A. Steiner, Phys. Rev. Lett. **85**, 2048 (2000) [arXiv:hep-ph/0005094].
- [5] M. Alford, P. Jotwani, C. Kouvaris, J. Kundu, and K. Rajagopal, arXiv:astro-ph/0411560.
- [6] M. Alford, K. Rajagopal, and F. Wilczek, Nucl. Phys. B **537**, 443 (1999) [arXiv:hep-ph/9804403].
- [7] T. Schäfer, Nucl. Phys. B **575**, 269 (2000) [arXiv:hep-ph/9909574]; N. J. Evans, J. Hormuzdiar, S. D. H. Hsu and M. Schwetz, Nucl. Phys. B **581**, 391 (2000) [arXiv:hep-ph/9910313]; D. K. Hong and S. D. H. Hsu, Phys. Rev. D **68**, 034011 (2003) [arXiv:hep-ph/0304156].
- [8] See, e.g., A. J. Leggett, Rev. Mod. Phys. **47**, 331 (1975); P. W. Anderson and W. F. Brinkman, in *The Physics of Liquid and Solid Helium, Part II*, edited by K. H. Bennemann and J. B. Ketterson (Wiley, New York, 1978), p. 177.
- [9] K. Iida and G. Baym, Phys. Rev. D **66**, 014015 (2002) [arXiv:hep-ph/0204124].
- [10] S. Reddy, M. Sadzikowski, and M. Tachibana, Nucl. Phys. A **714**, 337 (2003) [arXiv:nucl-th/0203011]; Phys. Rev. D **68**, 053010 (2003) [arXiv:nucl-th/0306015].
- [11] J. Kundu and S. Reddy, Phys. Rev. C **70**, 055803 (2004). [arXiv:nucl-th/0405055].
- [12] K. Iida and G. Baym, Phys. Rev. D **65**, 014022 (2002) [arXiv:hep-ph/0108149].
- [13] I. Giannakis and H. c. Ren, Nucl. Phys. B **669**, 462 (2003) [arXiv:hep-ph/0305235]; K. Iida, arXiv:hep-ph/0412426.
- [14] T. Matsuura, K. Iida, T. Hatsuda, and G. Baym, Phys. Rev. D **69**, 074012 (2004) [arXiv:hep-ph/0312042].
- [15] S. A. Chin, Annals Phys. **108**, 301 (1977).
- [16] S. Hands, J. B. Kogut, C. G. Strouthos, and T. N. Tran, Phys. Rev. D **68**, 016005 (2003) [arXiv:hep-lat/0302021]; S. Hands and C. G. Strouthos, arXiv:hep-lat/0406018.
- [17] L. D. Landau, Soviet Phys. JETP **5**, 101 (1957).
- [18] P. Wölfle, Phys. Rev. Lett. **31**, 1437 (1973); Phys. Rev. B **14**, 89 (1976).
- [19] G. Baym and S. A. Chin, Nucl. Phys. **A262**, 527 (1976).
- [20] V. P. Gusynin and I. A. Shovkovy, Nucl. Phys. **A700**, 577 (2002) [arXiv:hep-ph/0108175].
- [21] R. D. Pisarski and D. H. Rischke, Phys. Rev. D **60**, 094013 (1999) [arXiv:nucl-th/9903023].
- [22] K. Iida, T. Matsuura, M. Tachibana, and T. Hatsuda, Phys. Rev. Lett. **93**, 132001 (2004) [arXiv:hep-ph/0312363]; arXiv:hep-ph/0411356.
- [23] S. B. Ruster, I. A. Shovkovy, and D. H. Rischke, Nucl. Phys. A **743**, 127 (2004) [arXiv:hep-ph/0405170].
- [24] K. Fukushima, C. Kouvaris, and K. Rajagopal, arXiv:hep-ph/0408322.
- [25] M. Alford, C. Kouvaris, and K. Rajagopal, Phys. Rev. Lett. **92**, 222001 (2004) [arXiv:hep-ph/0311286]; arXiv:hep-ph/0406137.
- [26] K. Fukushima, Phys. Rev. D **70**, 094014 (2004) [arXiv:hep-ph/0403091].
- [27] M. Kitazawa, T. Koide, T. Kunihiro, and Y. Nemoto, Prog. Theor. Phys. **108**, 929 (2002) [arXiv:hep-ph/0207255].
- [28] A. Schmitt, Q. Wang, and D. H. Rischke, Phys. Rev. D **66**, 114010 (2002) [arXiv:nucl-th/0209050].
- [29] N. N. Bogoliubov, V. Tolmachev, and D. V. Shirkov, *New Method in the Theory of Superconductors* (Consultants Bureau, New York, 1959); P. W. Anderson, Phys. Rev. **112**, 1900 (1958).
- [30] T. Hatsuda and T. Kunihiro, Phys. Rev. Lett. **55**, 158 (1985).
- [31] K. Yokokawa, T. Hatsuda, A. Hayashigaki, and T. Kunihiro, Phys. Rev. C **66**, 022201 (2002) [arXiv:hep-ph/0204163]; A. Patkos, Z. Szep, and P. Szepfalusy, Phys. Rev. D **66**, 116004 (2002) [arXiv:hep-ph/0206040]; Y. Hidaka, O. Morimatsu, and T. Nishikawa, Phys. Rev. D **67**, 056004 (2003) [arXiv:hep-ph/0211015].
- [32] K. Zarembo, Phys. Rev. D **62**, 054003 (2000) [arXiv:hep-ph/0002123].
- [33] R. Casalbuoni and R. Gatto, Phys. Lett. B **464**, 111 (1999) [arXiv:hep-ph/9908227]; D. T. Son and M. A. Stephanov, Phys. Rev. D **61**, 074012 (2000) [arXiv:hep-ph/9910491]; D. K. Hong, T. Lee, and D. P. Min, Phys. Lett. B **477**, 137 (2000) [arXiv:hep-ph/9912531].
- [34] M. Rho, A. Wirzba, and I. Zahed, Phys. Lett. B **473**, 126 (2000) [arXiv:hep-ph/9910550]; M. Rho, E. V. Shuryak, A. Wirzba, and I. Zahed, Nucl. Phys. A **676**, 273 (2000) [arXiv:hep-ph/0001104].
- [35] M. Buballa, arXiv:hep-ph/0410397.
- [36] M. M. Forbes, arXiv:hep-ph/0411001.
- [37] A. A. Abrikosov, L. P. Gorkov, and I. E. Dzyaloshinski, *Methods of Quantum Field Theory in Statistical Physics* (Dover, New York, 1975).
- [38] I. J. R. Aitchison and D. J. Lee, Phys. Rev. B **56**, 8303 (1997); I. J. R. Aitchison, G. Metikas, and D. J. Lee, Phys. Rev. B **62**, 6638 (2000).
- [39] T. D. Lee and C. N. Yang, Phys. Rev. **113**, 1406 (1959); A. Griffin and E. Zarembo, Phys. Rev. A **56**, 4839 (1997).